PNAS RESEARCH ARTICLE | MICROBIOLOGY

AMP-dependent phosphite dehydrogenase, a phosphorylating enzyme in dissimilatory phosphite oxidation

Zhuqing Mao[a,b], Jennifer R. Fleming[a,b], Olga Mayans[a,b], Jasmin Frey[a], David Schleheck[a,b], Bernhard Schink[a,b,1], and Nicolai Müller[a,1]

Edited by Caroline Harwood, University of Washington, Seattle, WA; received June 14, 2023; accepted September 20, 2023

Oxidation of phosphite (HPO_3^{2-}) to phosphate (HPO_4^{2-}) releases electrons at a very low redox potential (E_0 = −690 mV) which renders phosphite an excellent electron donor for microbial energy metabolism. To date, two pure cultures of strictly anaerobic bacteria have been isolated that run their energy metabolism on the basis of phosphite oxidation, the Gram-negative *Desulfotignum phosphitoxidans* (DSM 13687) and the Gram-positive *Phosphitispora fastidiosa* (DSM 112739). Here, we describe the key enzyme for dissimilatory phosphite oxidation in these bacteria. The enzyme catalyzed phosphite oxidation in the presence of adenosine monophosphate (AMP) to form adenosine diphosphate (ADP), with concomitant reduction of oxidized nicotinamide adenine dinucleotide (NAD^+) to reduced nicotinamide adenine dinucleotide (NADH). The enzyme of *P. fastidiosa* was heterologously expressed in *Escherichia coli*. It has a molecular mass of 35.2 kDa and a high affinity for phosphite and NAD^+. Its activity was enhanced more than 100-fold by addition of ADP-consuming adenylate kinase (myokinase) to a maximal activity between 30 and 80 mU x mg protein^{-1}. A similar NAD-dependent enzyme oxidizing phosphite to phosphate with concomitant phosphorylation of AMP to ADP is found in *D. phosphitoxidans,* but this enzyme could not be heterologously expressed. Based on sequence analysis, these phosphite-oxidizing enzymes are related to nucleotide-diphosphate-sugar epimerases and indeed represent AMP-dependent phosphite dehydrogenases (ApdA). A reaction mechanism is proposed for this unusual type of substrate-level phosphorylation reaction.

substrate-level phosphorylation | ADP formation | *Phosphitispora fastidiosa* | *Desulfotignum phosphitoxidans* | early biochemical evolution

Significance

We describe here an unusual substrate-level phosphorylation with phosphite as an inorganic electron donor. Two strains of strictly anaerobic bacteria have been isolated so far which use the low-potential electrons of phosphite oxidation in their energy metabolism. The enzyme oxidizes phosphite with concomitant phosphorylation of AMP (adenosine monophosphate) to ADP (adenosine diphosphate) and reduction of NAD^+ (oxidized nicotinamide adenine dinucleotide). Although phosphites today make up only a minor fraction of phosphorus minerals, they were probably far more important in the early era of biochemical evolution. This type of substrate-level phosphorylation covers the major part of energy conservation in these bacteria and might represent a remnant of early biochemical evolution when phosphite was more abundant in the biosphere than it is today.

Phosphorus (P) is an essential element for the metabolism of all life forms. It was isolated first from human urine in 1669 (1) and makes up 0.09% by mass of the Earth's crust (2). Due to its high reactivity, phosphorus is never found as a free element in nature but occurs as inorganic phosphate, phosphite, hypophosphite, phosphine, as well as phosphate esters and organic phosphonates containing C–P linkages. Phosphates (PO_4^{3-}) are the most stable and the most important phosphorus compounds on Earth and are essential constituents of DNA, RNA, ATP (adenosine triphosphate), ADP (adenosine diphosphate), AMP (adenosine monophosphate), phospholipids, etc.; there is no life without phosphate (3–5). Beyond phosphate, recently, phosphite (PO_3^{3-}) has been detected at low levels in aquatic ecosystems such as oceans, lakes, rivers, and sewage treatment plants (6). Phosphite was probably more abundant in the Archean period when the Earth's crust was less oxidized than today and played perhaps a key role in the early evolution of life (3, 7–9). Phosphite is formed naturally by lightning and volcanic eruptions (10); it is also produced industrially as a constituent of fertilizers and pesticides (11, 12). Treatment of crop seeds with phosphite fertilizers can increase production yields, and phosphite production is expanding gradually with its possible application in agriculture (13).

Under phosphate limitation, several bacteria can use phosphite as an alternative phosphorus source (14). This assimilatory phosphite oxidation was described first in 1953 (15). For a *Pseudomonas* strain (16), an NAD^+-dependent phosphite dehydrogenase was enriched and characterized (17, 18). For a *Bacillus caldolyticus* strain, also the use of further reduced inorganic phosphorus sources was reported, and this capacity was attributed to a hypophosphite oxidase which oxidized both hypophosphite and phosphite to orthophosphate (19). Phosphite assimilation was further reported for an anaerobic *Bacillus* strain (20). More detailed studies on the assimilation of reduced phosphorus compounds were carried out with *Escherichia coli* (21), *Pseudomonas stutzeri* (14), and *Klebsiella aerogenes* (22). In these bacteria, oxidation of phosphite to phosphate is catalyzed by an NAD^+-dependent phosphite dehydrogenase (PtxD) which was heterologously expressed in *E. coli*, purified, and characterized in detail (23). Phosphite oxidation with NAD^+ by this enzyme is an irreversible reaction due to the low redox potential of phosphite oxidation (E_0 = −690 mV) compared to that of the NAD^+/NADH couple (−320 mV). This enzyme

Author contributions: J.F., D.S., B.S., and N.M. designed research; Z.M., J.R.F., O.M., and N.M. performed research; Z.M., J.R.F., O.M., J.F., D.S., and N.M. analyzed data; and Z.M., J.R.F., O.M., J.F., D.S., B.S., and N.M. wrote the paper.

The authors declare no competing interest.

This article is a PNAS Direct Submission.

[1]To whom correspondence may be addressed. Email: bernhard.schink@uni-konstanz.de or nicolai.mueller@uni-konstanz.de.

This article contains supporting information online at https://www.pnas.org/lookup/suppl/doi:10.1073/pnas.2309743120/-/DCSupplemental.

Published November 3, 2023.

is specific for phosphite as an electron donor and is related to D-2-hydroxyacid dehydrogenases. Three different mechanisms for this reaction have been discussed so far, of which two involve an initial nucleophilic attack of NAD^+ on the phosphorus atom and subsequent hydride transfer. The third one includes a primary hydride transfer from phosphite to NAD^+; this mechanism appears to be substantiated by kinetic data (24). Moreover, an alkaline phosphatase was described for *E. coli* which can also act as a phosphite-dependent hydrogenase (25).

Phosphite could also be an excellent electron donor for microbial energy metabolism. A first dissimilatory phosphite-oxidizing bacterium, the strictly anaerobic *Desulfotignum phosphitoxidans* FiPS-3^T was isolated from marine sediment (26, 27) and oxidizes phosphite to phosphate with simultaneous reduction of sulfate to sulfide, or with homoacetogenic reduction of CO_2 to acetate. The phosphite oxidation capacity of this bacterium appeared to be associated with four genes (*ptxD-ptdFCG*) which when transferred to a phosphite-oxidation negative acceptor bacterium conferred assimilatory phosphite oxidation but did not allow for the use of phosphite as an electron donor for chemolithotrophic growth (28). A further strictly anaerobic dissimilatory phosphite-oxidizing bacterium, *Phosphitispora fastidiosa* DYL19^T, was isolated recently from anaerobic sludge of a sewage treatment plant (29). It uses only phosphite as the electron donor and carbon dioxide as the electron acceptor in its energy metabolism; no alternative substrates are known (29). Comparably high growth yields of these cultures with phosphite indicated that they can efficiently exploit the bioenergetic potential of phosphite oxidation, and a direct linkage between phosphite oxidation and ATP synthesis was anticipated by Wolfgang Buckel (30). Dissimilatory phosphite oxidation has been described also for some anaerobic enrichment cultures (31, 32).

In the present paper, we describe enzyme assays, heterologous expression, purification, and characterization of AMP-dependent phosphite dehydrogenases (ApdA) in *P. fastidiosa* and *D. phosphitoxidans* which combine AMP- and NAD^+-dependent phosphite oxidation with the conservation of metabolic energy by formation of an energy-rich phosphoanhydride linkage, thus catalyzing a substrate-level phosphorylation.

Results

Phosphite-Dependent NAD^+ Reduction in Cell-Free Extracts of *D. phosphitoxidans* and *P. fastidiosa* Is Stimulated by Addition of AMP. Spectrophotometric assays for phosphite-oxidizing enzyme activity were carried out with cell-free extracts of *D. phosphitoxidans* FiPS-3 and *P. fastidiosa* DYL19 grown with phosphite as the sole electron donor. We applied strictly anoxic conditions throughout cell harvest, cell-extract preparation, and enzyme assays. Phosphite-dependent acceptor reduction was observed only with NAD^+ as the electron acceptor (33). Alternative electron acceptors such as methyl viologen, benzyl viologen, flavin mononucleotide, flavin adenine dinucleotide, or phenazine methosulfate were not reduced. Specific phosphite-dependent NAD^+ reduction was slightly higher in extracts of *P. fastidiosa* (4.9 ± 0.4 mU x mg protein^{-1}) than in extracts of *D. phosphitoxidans* (1.88 ± 0.3 mU x mg protein^{-1}). Addition of AMP enhanced the activity by 63 and 88%, respectively. ADP and ATP addition inhibited the activity by about 50% and up to 100%, respectively. UMP stimulated the reaction in a manner similar to AMP; UDP and UTP inhibited the reaction. GMP, TMP, pyruvate, acetate, sodium sulfide, coenzyme A, coenzyme M, serine, cysteine, hydroxocobalamine, and thiamine diphosphate as cofactors had no influence on the rate of phosphite-dependent NAD^+ reduction (33).

Identification of a Candidate Phosphite-Oxidizing Enzyme in *P. fastidiosa*. To search for enzymes involved in phosphite-driven energy metabolism of *P. fastidiosa* cells, its proteome after growth with phosphite was analyzed in cell-free extracts; lack of an alternative energy substrate for *P. fastidiosa* did not allow for a differential proteomics approach. In the proteomics data, the abundance of a protein is represented as the corresponding cumulative peak-area of its peptides identified by mass spectrometry. Area values of six biological replicates (n = 6) were sorted by descending order (Dataset S1). In all cases, a protein that had been automatically annotated as NAD(P)-dependent oxidoreductase and nucleoside-diphosphate-sugar epimerase-family protein (NAD^+-dependent epimerase/dehydratase family, PF01370) (IMG gene ID 2888954517) was the most abundant protein, as illustrated in Fig. 1*A* by the average total-peak area of all identified peptides for all six replicates. It has a predicted molecular weight of 35.198 kDa (see below). Enzymes of the Wood–Ljungdahl pathway were also highly abundant (Fig. 1*A*). An interesting candidate for interconversion of adenine nucleotides, an adenylate kinase (myokinase, IMG gene ID 2888951025), was highly expressed, as the top-17th most abundant protein as judged by the average peak area (Fig. 1*A*).

We next evaluated the soluble protein extract of *P. fastidiosa* by denaturing protein electrophoresis [SDS-PAGE (sodium dodecyl sulfate polyacrylamide gel electrophoresis)] for its most prominent proteins (Fig. 1*B*). The most prominent band was visible at about 36-kDa molecular weight, and it was excised and submitted to proteomics analysis, which identified the above-mentioned nucleoside-diphosphate-sugar epimerase family protein (IMG gene ID 2888954517) (Dataset S2). For staining of phosphite-oxidizing enzyme activity, the native gel after electrophoresis was transferred into an anoxic tube and incubated with phosphite as the electron donor, NAD^+ as the intermediate electron carrier, and iodonitrotetrazolium chloride (INT) as the terminal electron acceptor to form a purple formazan dye. A slightly stained band (*SI Appendix*, Fig. S1*A*) was excised and analyzed by proteomics, which again identified the nucleoside-diphosphate-sugar epimerase family protein mentioned above (IMG gene ID 2888954517) as one of the most prominent proteins present (Dataset S3). A homolog of this protein has previously been identified as specifically and most strongly expressed protein during growth of *D. phosphitoxidans* FiPS-3 with phosphite as the electron donor (34) (IMG gene ID 2523425543 /2515197609), though its function and role in phosphite-driven energy metabolism remained unclear (27, 28, 34, 35). This protein represented the most prominent band visible after SDS-PAGE of cell-free extract of phosphite-grown *D. phosphitoxidans* at about 38 kDa (Fig. 1*B*) (see also refs. 27 and 34), as confirmed by proteomics (Dataset S4). In addition, after native-PAGE and activity staining, a slightly stained band was visible (*SI Appendix*, Fig. S1*B*), which was excised and also confirmed by proteomics to contain the nucleoside-diphosphate-sugar epimerase family protein as the most prominent protein (Dataset S5).

Heterologous Expression and Activity of the Candidate Phosphite-Oxidizing Enzyme of *P. fastidiosa*. The genes from both bacteria were cloned each into the expression plasmid pET-28a(+) in-frame with the N-terminal His_6-tag included in pET-28a(+). After growth and induction with IPTG or cultivation in autoinduction medium, no protein was produced by several tested *E. coli* expression strains with the construct carrying the gene of *D. phosphitoxidans*. In contrast, the synthetic gene for the nucleoside-diphosphate-sugar epimerase-like protein of *P. fastidiosa* with a molecular mass of 37.7 kDa including the His_6-tag was successfully

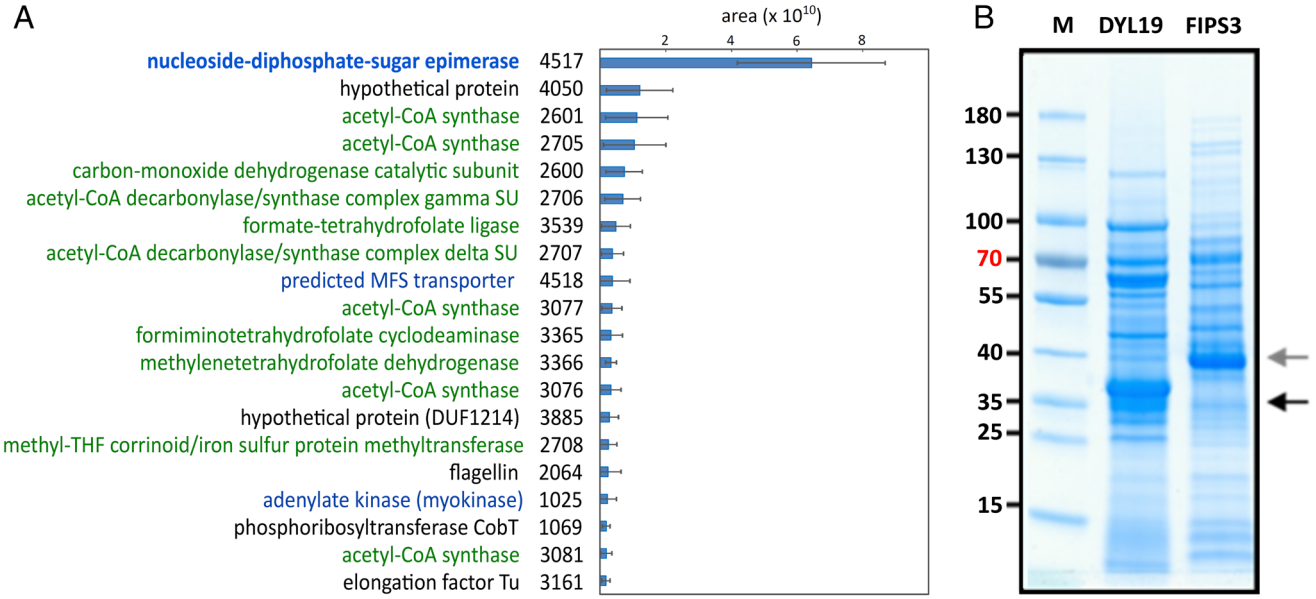

Fig. 1. Excerpt of total proteomics data for cell-free extract of *D. fastidiosa* DYL19 grown with phosphite (*A*) and SDS-PAGE gel (*B*) for cell-free extracts of strain DYL19 and of *D. phosphitoxidans* FiPS-3 grown with phosphite. (*A*) The top 20 most abundant proteins are shown, with protein abundance evaluated by the corresponding cumulative peak-area of their peptides identified by mass spectrometry. The error bars indicate SDs calculated for six replicates (n = 6) of individually grown DYL19 cultures. The four-digit gene numbers used (locus tags) are referring to the IMG annotation of the *D. fastidiosa* DYL19 genome; the IMG gene-ID prefix 288895xxxx has to be included for accessing the gene information (https://img.jgi.doe.gov/cgi-bin/m/main.cgi?section=GeneSearch). A predicted nucleoside-diphosphate-sugar epimerase protein (IMG gene ID 2888954517) was indicated as the most abundant protein (bold blue) in the cell-free extracts. Enzymes of the Wood–Ljungdahl pathway were among the highest abundant proteins (indicated in green) as well as a predicted adenylate kinase (myokinase) protein (1,025) (see main text and Dataset S1). A predicted MFS transporter gene (4,518) coencoded in the same gene cluster with the predicted nucleoside-diphosphate-sugar-epimerase gene (*SI Appendix*, Fig. S11) was also highly expressed (Dataset S1). (*B*) Proteins in cells-free extracts were separated by denaturing SDS-PAGE against molecular weight markers (*Left*, in kDa). Each most prominent band was excised and submitted to proteomic analysis (see main text). The black arrow points at the most prominent band excised for *D. fastidiosa* and the gray arrow at the most prominent band excised for *D. phosphitoxidans*.

produced and could be purified to near homogeneity. The protein preparations and enzyme assays were initially done under strictly anoxic conditions until we later realized that the enzyme was not sensitive to oxygen (see below). The protein preparations still contained several contaminating proteins of *E. coli* (*SI Appendix*, Fig. S2). To avoid protein precipitation, addition of 10% (v/v) glycerol to all buffers used for purification was necessary.

Activity of the recombinant protein was first tested in spectrophotometric enzyme assays by monitoring NADH production upon addition of phosphite. When measured with cell-free extracts of the *E. coli* strain producing the *P. fastidiosa* enzyme, the reaction exhibited a high affinity for phosphite (app. K_m = 0.059 mM) and for NAD^+ (app. K_m = 0.024 mM). There was no epimerase activity with UDP glucose and NAD^+ detectable, compared with cell-free extract prepared from noninduced and nonproducing *E. coli*. Specific activities of the purified recombinant protein in the absence or presence of AMP, NAD^+, phosphite, and/or the absence or presence of auxiliary ADP-consuming enzymes such as myokinase (see also below), were assayed under anoxic conditions, as shown in Fig. 2*A* for a representative enzyme preparation. Highest activity (here, 29.1 ± 1.1 mU x mg $protein^{-1}$) was observed only if active recombinant enzyme (ApdA), NAD^+, AMP, phosphite, and myokinase as auxiliary enzyme were combined in one assay, whereas the activity without myokinase was lower than in control experiments without phosphite or AMP (Fig. 2*A*). In control assays without phosphite, an initial background activity was observed, which ceased to 3.3 ± 1 mU/mg (yellow bar, Fig. 2*A*) after around 500 s, but increased to full activity after addition of phosphite. Similar observations were made in control assays without AMP (light blue bar, Fig. 2*A*). The latter two results were interpreted as background activities in assays with myokinase. When heat-inactivated ApdA was added to assay mixtures, a slight decrease in absorption was observed which was attributed to sedimentation of precipitated, denatured protein (Fig. 2*A*).

With $NADP^+$ instead of NAD^+, the specific activity was reduced by 99% (0.74 ± 0.08 versus 79.3 ± 8.6 mU x mg $protein^{-1}$, as measured for a different enzyme preparation in the presence of myokinase). Further, with ADP instead of AMP, the activity was reduced by 97% (1 ± 0.18 versus 29.1 ± 1.1 mU x mg $protein^{-1}$) and with UMP instead of AMP by 98% (0.05 ± 0.06 mU x mg $protein^{-1}$). Hence, AMP was the only nucleoside phosphate known which supported the enzyme activity. Therefore, the enzyme was termed ApdA.

Purified recombinant ApdA maintained its activity also when the enzyme was purified and stored under oxic conditions; therefore, all subsequent assays were done under air. The activity was stable under air for at least 48 h, no matter whether it was stored at 4 °C or −20 °C; at room temperature, a decrease of activity by about 20% and protein precipitation was observed (*SI Appendix*, Fig. S3).

For oxic enzyme assays with recombinant ApdA and myokinase as auxiliary enzyme, ATP formation could be detected qualitatively by coupling the reaction with luciferase (Fig. 2*B*). Only in assays with 1 mM NAD^+, 1 mM AMP, 5 mM phosphite, 100 to 125 µg ApdA, and 20 units myokinase and luciferase, an increase in chemiluminescence up to 55,000 relative luminescence units (RLU) was observed within 62 min. Various control assays, in which at least one of the assay components was omitted, showed no significant increase in chemiluminescence (Fig. 2*B*).

Testing Alternative Auxiliary Enzymes. As described above, when ApdA was assayed without myokinase, only little activity was detectable as measured via NADH-formation (0.5 ± 0.3 mU/mg, see Fig. 2*A*), while in the presence of myokinase, ApdA activities

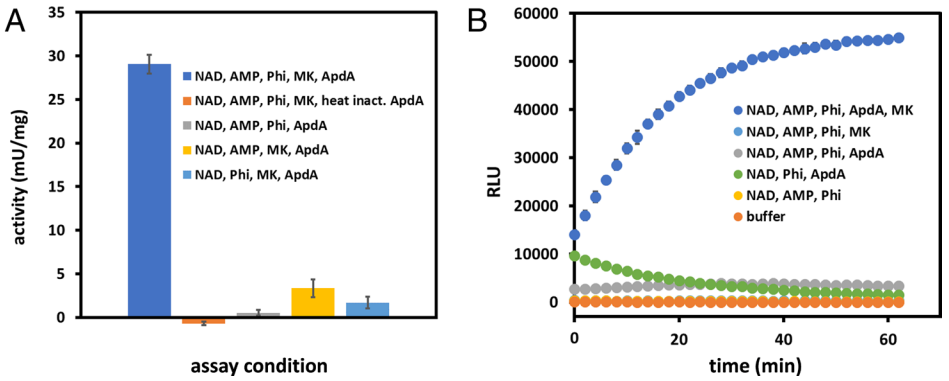

Fig. 2. Activities of heterologously overproduced nucleoside-diphosphate-sugar epimerase (ApdA) of *P. fastidiosa*. (*A*) Anoxic photometric enzyme assays of phosphite-dependent NAD^+ reduction. The substrate concentrations used were 10 mM phosphite, 2 mM NAD^+, and 2 mM AMP. Shown are mean values ± SD of triplicates. (*B*) Chemiluminescence assay with controls. The ApdA reaction coupled to myokinase was further coupled to firefly luciferase, showing an increase of chemiluminescence at 560 nm. Shown are mean values ± SD of triplicates; most error bars are smaller than symbol size. Abbreviations used: Phi, phosphite; MK, myokinase; RLU, relative luminescence units.

were in the range of 30 to 80 mU x mg $protein^{-1}$ for the different recombinant enzyme preparations, thus around 100-fold higher than the ApdA activity in the absence of myokinase. When ApdA was assayed with pyruvate kinase as an alternative ADP-consuming enzyme [in the presence of phosphoenolpyruvate (PEP) as the substrate in reverse] or hexokinase as an ATP-consuming enzyme (in the presence of glucose), activities were 2.5 ± 1.1 mU x mg $protein^{-1}$ and 4.3 ± 0.2 mU x mg $protein^{-1}$, respectively. Hence, myokinase could not be replaced by these enzymes. When both myokinase and hexokinase (plus glucose) were added, the activity was 97 ± 2 mU x mg $protein^{-1}$, thus appeared to be higher than with myokinase alone. In addition, the absorption change with myokinase as the sole auxiliary enzyme was linear only within the first 50 s after reaction start and decelerated afterward (*SI Appendix*, Fig. S4*A*), while in assays with both myokinase as ADP-consuming and hexokinase as an additional ATP-consuming enzyme, the absorption change was linear over more than 400 s until a final absorption higher than 1 was reached (*SI Appendix*, Fig. S4*B*).

Discontinuous Enzyme Assays with ApdA of *P. fastidiosa*. ApdA reactions were followed in discontinuous enzyme assays in which samples were taken at intervals from the reaction mixture and the substrate conversion and product formation were analyzed by HPLC. In assays without myokinase and each 20 mM phosphite, NAD^+ and AMP as substrates, formation of peaks corresponding to ADP and ATP was detectable after several hours of incubation (*SI Appendix*, Fig. S5); however, only a net accumulation of 57.3 µM ADP over 6 h could be quantified, as well as of 13.6 µM ATP; the specific activity determined via the ADP formation was 70.8 ± 2.8 µU/mg $protein^{-1}$ (*SI Appendix*, Fig. S6). Note that disappearance of substrates could not be quantified in these experiments by HPLC due to their high concentrations and thus detector overload.

In discontinuous assays using 10 mM phosphite, 2 mM NAD^+, and 2 mM AMP in the presence of myokinase, 0.6 mM NADH was produced within 5 h (Fig. 3*A*), while in assays with both myokinase and hexokinase, 1.7 mM NADH was produced in the same time (Fig. 3*B*). Simultaneously, ADP accumulated to 1.6 mM concentration within 5 h while almost no ATP was detected in assays with both myokinase and hexokinase (Fig. 3*B*). In the presence or absence of hexokinase, 2.2 mM phosphite was consumed. Conversion of 0.5 mM AMP within 5 h could be observed only in assays with myokinase as the sole auxiliary enzyme (Fig. 3*A*). In assays with myokinase as the sole auxiliary enzyme, accumulation of an unidentified anionic compound was observed in IEX-HPLC. Its retention time (11.1 min) was closest to that of hypophosphite (11.3 min), but this compound could not yet be identified (*SI Appendix*, Fig. S7). For analytical reasons, phosphate and hypophosphite could not be measured in assays with both myokinase and hexokinase. Pyrophosphate (retention time 7.7 min, shortly after the injection peak) was never found as a reaction product. Assays without phosphite showed no disappearance of substrates or formation of products (*SI Appendix*, Fig. S8).

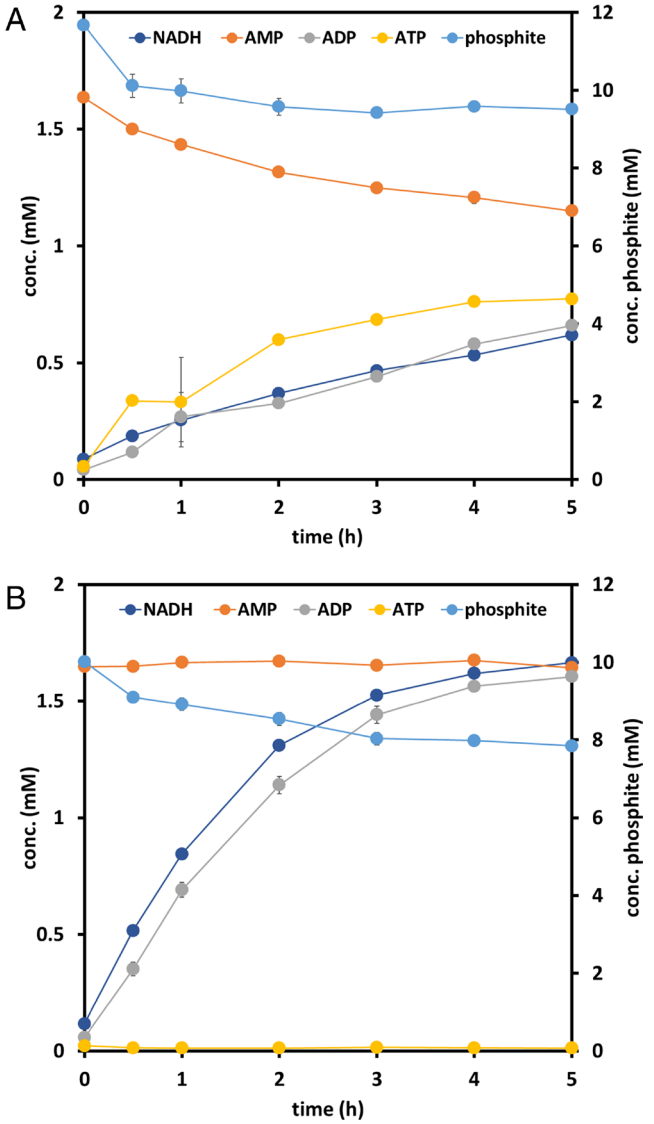

Fig. 3. Discontinuous enzyme assays with ApdA of *P. fastidiosa* and myokinase. (*A*) The 2 mL assay mixture in 25 mM HEPES-KOH, pH 8.0, 3 mM $MgCl_2$ contained 2 mM NAD^+, 2 mM AMP, 10 mM phosphite, 20 units myokinase, and 409 µg of recombinant purified ApdA. (*B*) The 2 mL assay mixture in 25 mM HEPES-KOH, pH 8.0, 3 mM $MgCl_2$ contained 2 mM NAD^+, 2 mM AMP, 10 mM phosphite, 20 units myokinase, 20 mM glucose, 20 units hexokinase, and 409 µg ApdA. Shown are mean values ± SD of triplicates. Some error bars are smaller than symbol size.

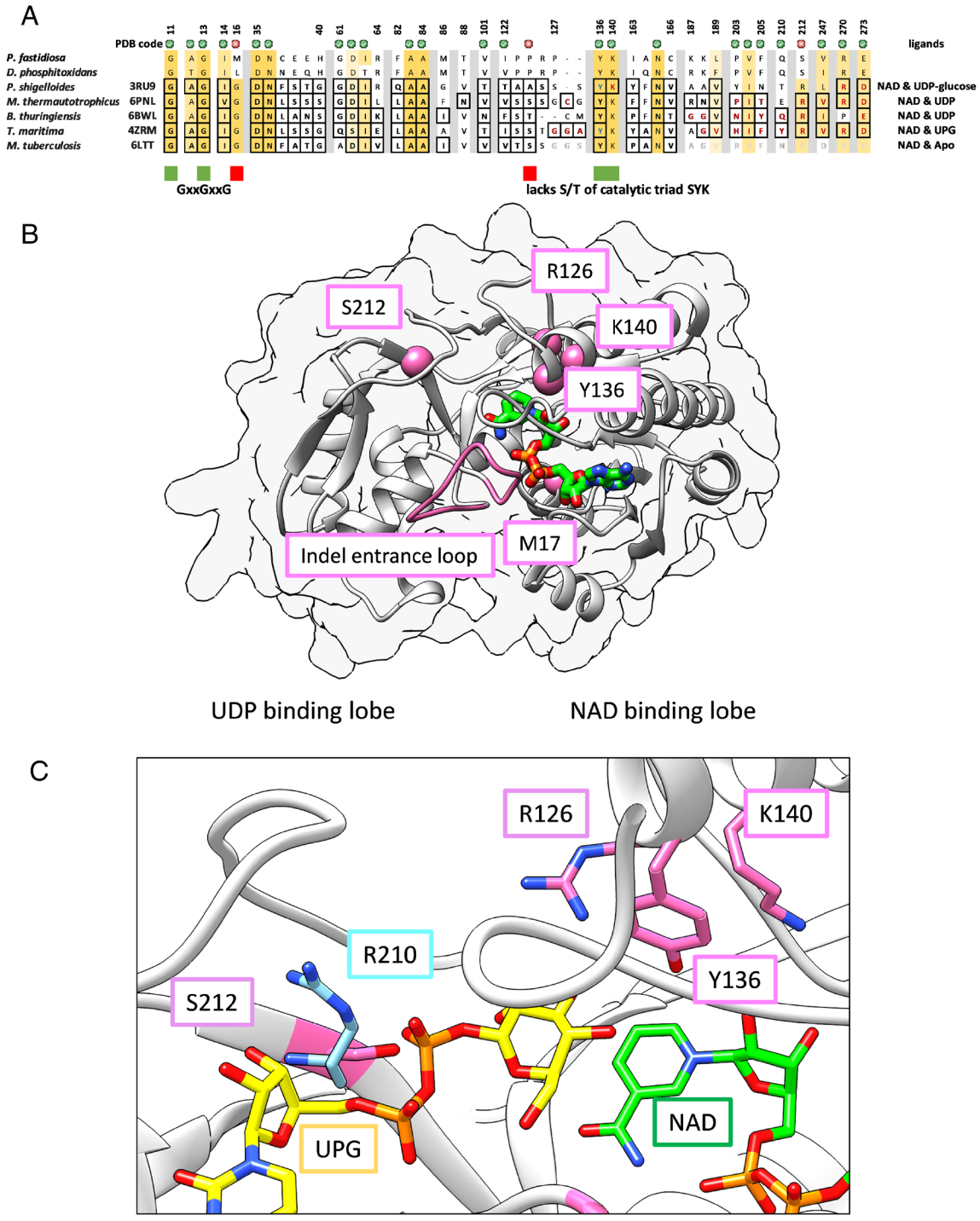

Fig. 4. Bioinformatic analysis of ApdA enzymes of *P. fastidiosa* and *D. phosphitoxidans*. (*A*) *P. fastidiosa* and *D. phosphitoxidans* ApdA enzymes aligned to their five closest homologs with known structures. Residue numbering by *P. fastidiosa* sequence. Colors indicate the degree of similarity: dark yellow, 100% conservation; medium yellow, conservation between groups of strongly similar properties; light yellow- conservation between groups of weakly similar properties. Binding residues (boxed) defined by PDB sequence annotations: NAD^+-binding residues are shown in black bold, and nucleotide phosphate (UDP or UPG) binding residues (type indicated far right) are shown in red bold letters. Dual binders are shown in blue. *M. tuberculosis* residues are shown in gray, where it is not possible to assess nucleotide phosphate binding as the sugar pocket is in the apo state. A green dot above a residue position indicates that the residue in both ApdA enzymes is found in one of the homologous sequences. A red dot highlights the variant residue in the nucleotide phosphate-binding site. (*B*) *Pf*APD AlphaFold model. The crystal structure 4ZRN was structurally aligned and NAD^+ shown as sticks. Residues discussed in the text are shown as pink spheres. The substrate binding site indel loop is in pink. (*C*) Overview of the catalytic core. Residues in text shown as sticks colored as in *A*. UDP-glucose (UPG) from 4ZRN (yellow) and residue R222 (blue) are shown as sticks colored by heteroatom.

Sequence Analysis and a Structural 3D Model of *P. fastidiosa* ApdA. ApdA of *P. fastidiosa*, and its close homolog in *D. phosphitoxidans*, are homologous to members of the large short-chain dehydrogenases/reductases (SDR) family of NAD(P)-dependent oxidoreductases and nucleotide-sugar 4-epimerases (~35 to 60% sequence identity). Typically, these enzymes perform epimerization reactions on sugar substrates. For nucleotide-sugar 4-epimerases, this usually involves changing UDP-glucose to UDP-galactose, an intramolecular oxidation-reduction reaction, as a pivotal step in D-galactose metabolism (36). Alignment of the ApdA sequences with their

five closest homologues with known 3D structures (Fig. 4), which are all UDP-binding epimerases, revealed high conservation, particularly in regions involved in substrate binding (e.g., *Pf*ApdA and *Mycobacterium tuberculosis* UDP-glucose 4-epimerase GalE1 share 32% seq. id.; *Thermotoga maritima* UDP-Glucose 4-Epimerase, 32% seq. id.; *B. thuringiensis* Pal, 31% seq. id.; *Methanothermobacter thermautotrophicus* UDP-GalNAc 4-epimerase, 26% seq. id.; and *Plesiomonas shigelloides* UDP-GalNAc 4-epimerase, 28% seq. id.).

There were, however, three significant sequence differences observed in substrate binding groups (Fig. 4*A*, red sphere). These are *i*) residue (M/L) in position 16 of the ApdA of *P. fastidiosa* within the glycine-rich GxxGxxG motif involved in NAD^+ binding, which in other sequences is a G (36); *ii*) absence of the catalytic serine in the canonical SYK triad (36), which in this case is substituted for P; and *iii*) a serine (position 212 in *Pf*ApdA) instead of the typical arginine involved in β-phosphate coordination of the UDP-sugar substrate (37).

To better understand the possible functional consequences of these residue exchanges, structural 3D models of both ApdA enzymes were calculated using AlphaFold2 (38) (*SI Appendix*, Fig. S9) and the sequence differences compared in a structural context. The similarity of their sequences (seq. id. 62%) was reflected in the high similarity of their predicted 3D-folds ($RMSD_{C\alpha}$ = 0.56 Å). The models were then superimposed onto the top five structural homologues (*SI Appendix*, Fig. S10), allowing for a comparison of sequence differences within a structural context. The 3D-fold of NAD(P)-dependent oxidoreductases and nucleotide-sugar 4-epimerase enzymes of the SRD family comprises two lobes, with the active site at their center. The N-terminal lobe, which binds NAD^+, is highly conserved across prokaryotes and eukaryotes (37). The high conservation of the fold and its NAD^+-binding residues allowed us to model the binding of NAD^+ by the ApdAs with high reliability. In both enzymes, the characteristic GxxGxxG motif that binds the phosphate groups of NAD^+ is degenerated to GxxGxx(M/L) (Fig. 4*A*). Despite its strict conservation in the top 100 homologues of ApdA, the third glycine is located away from the NAD^+ binding site (Fig. 4*B*, blue sphere) and does not directly interact with the cofactor. Therefore, the functional consequence of a variant in this position, if any, is unclear. The N-terminal lobe typically contains a characteristic SYK catalytic triad (located in loop 122 to 127 of *Pf*ApdA). However, both ApdAs have an incomplete triad, retaining the YxxxK residues, but with the serine being substituted by a proline (Fig. 4*A*). The absence of the triad's serine may explain the observed lack of epimerase activity in the ApdAs. In *E. coli* GalE, the mutation of this serine to alanine reduces its epimerase activity almost 3,000-fold (39). However, some family members lacking this residue still exhibit catalytic activity, such as WbmF from *Bordetella bronchiseptica* (PDB 2Q1T), which has an alanine residue in this position (Fig. 4*A*) (40). However, WbmF is speculated to catalyze a 3,5-epimerization reaction instead of 4-epimerization. Interestingly, the ApdA models show the presence of an arginine (R126) close to the absent catalytic serine (Fig. 4*B*, pink sphere behind yellow spheres), near the catalytic tyrosine. This arginine could potentially contribute to the divergent catalytic activity of these enzymes. The C-terminal lobe, in structural homologues of known function, is associated with UDP-sugar binding, typically glucose or galactose. UDP binding residues (Fig. 4*A*, red residues) are highly conserved in the two ApdA enzymes and their homologues, except at position 212 (*Pf*ApdA residue numbering). In ApdA, this position contains a serine, whereas homologous sequences exhibit a conserved arginine (83% of the top 100 BLAST hits; 33 homologues with known structures). This arginine coordinates the β-phosphate of the UDP/UDP-sugar; in ApdAs, it may contribute to an altered substrate specificity. Furthermore, residues N176-E184 in the C-terminal lobe (Fig. 4*B*, pink loop) form an extended indel, which is variable in other homologues, and may play a role in substrate selectivity or binding regulation.

Discussion

In the present paper, we describe a phosphite-oxidizing enzyme that couples the oxidation step with substrate-level phosphorylation, to form an energy-rich phosphoanhydride bond. The free energy available from the electron transfer from the phosphate/phosphite couple (E_0' = −690 mV) to the NAD^+/NADH couple (E_0' = −320 mV) is $\Delta G_0'$ = −71.4 kJ per mol; this is more than sufficient to form under physiological conditions a phosphoanhydride bond as present in, e.g., ADP or ATP (41). The enzyme catalyzing this type of phosphite-dependent formation of ADP from AMP is present in both strains of anaerobic bacteria that have been described so far to be capable of dissimilatory phosphite oxidation, i.e., the gram-negative *D. phosphitoxidans* (26, 27) and the gram-positive *P. fastidiosa* (29). The ApdA protein of *D. phosphitoxidans* has been identified earlier as the most prominent, inducibly expressed protein during growth with phosphite as the electron donor (34), as well as an alternative NAD-dependent phosphite dehydrogenase encoded in the same gene cluster (PtxD; see *SI Appendix*, Fig. S11 and ref. 28). In the light of the results of this study, we consider it most likely that the PtxD of *D. phosphitoxidans* represents an assimilatory phosphite dehydrogenase homologous to the one of *P. stutzeri* WM 88 (23), which was detectable also in the proteome of *P. fastidiosa* at very low abundance (as the 716th most abundant protein; Dataset S1). Candidate ApdA genes were found in a metagenome-assembled genome (MAG) that was obtained from a community enriched for phosphite oxidation coupled to CO_2 reduction (31), as well as in two MAGs of *Bradyrhizobium* spp. (*SI Appendix*, Fig. S11). These ApdA candidates are also coencoded with homologs of the MFS-transporter gene that is highly expressed in *P. fastidiosa* (Fig. 1*A*) as well as with candidate genes for PtxD (*SI Appendix*, Fig. S11).

Total proteome analysis of *P. fastidiosa* indicated that ApdA is the most abundant enzyme in phosphite-grown cells and that also myokinase (adenylate kinase) is present at overaverage abundance. Remarkably, the phosphite-dependent NAD^+-reducing activity of ApdA can be measured at high rates only in the presence of ADP-consuming myokinase, or myokinase plus ATP-consuming hexokinase, or myokinase plus ATP-consuming luciferase (see reaction equations below). Assays with pyruvate kinase or hexokinase alone exhibited much lower activity. For myokinase from yeast, the K_M values K_{ADP} = 0.27 mM and K_{ATP} = 0.054 mM were reported (42), and the K_M values of pyruvate kinase from rabbit muscle and hexokinase from yeast are K_{ADP} = 0.357 mM and K_{ATP} = 0.063 mM, respectively (43, 44). Thus, differences in the K_M of these enzymes cannot explain the different activities of these auxiliary enzymes when coupled to ApdA. Moreover, ADP can accumulate during the ApdA plus myokinase reactions (Fig. 3*A*), and, hence, ADP does not appear to inhibit the ApdA reaction per se. One explanation may be that myokinase needs to interact spatially with ApdA, for example, to withdraw the reaction product directly from its catalytic site.

The equations for the different enzyme reactions involved in this study can be considered as follows:

$$\text{myokinase: } 2\ \text{ADP} \leftrightarrow \text{AMP} + \text{ATP}, \quad [1]$$

both ADP and ATP can be released from the ApdA enzyme, with ADP as the predominant product. In the assays with myokinase as the coupling enzyme, disappearance of AMP concomitant with formation of ADP and ATP was observed (Fig. 3*A*) as expected, but the reason why the AMP concentration did not change in our assays with both myokinase and hexokinase remains unclear. It can be expected that a proportion of ADP will be converted back to AMP by myokinase; however, an overall decrease of AMP should be detectable as ADP and ATP were formed as the final products of the reaction (Fig. 3*B*). These so-far unbalanced stoichiometries in our enzyme assays remain enigmatic until further experimental elucidation. They may be explained for example by yet uncharacterized side reactions of the up to three different enzymes in these assay systems or the effect of reaction products, but also of salts concentration or of pH, on the state of the myokinase equilibrium.

$$\text{pyruvate kinase: phosphoenolpyruvate} + \text{ADP} \rightarrow \text{pyruvate} + \text{ATP}, \quad [2]$$

$$\text{hexokinase: glucose} + \text{ATP} \rightarrow \text{glucose} - 6 - \text{phosphate} + \text{ADP}, \quad [3]$$

$$\text{luciferase: ATP} + \text{luciferin} + O_2 \rightarrow \text{AMP} + \text{oxyluciferin} + \text{pyrophosphate} + CO_2 + \text{light}, \quad [4]$$

$$\text{ApdA} + \text{myokinase: } 2\ \text{AMP} + 3\,NAD^+ + 3\ \text{phosphite} \rightarrow \text{ADP} + \text{ATP} + 3\ \text{NADH}, \quad [5]$$

$$\text{ApdA} + \text{myokinase} + \text{hexokinase: } 2\ \text{AMP} + 3\ NAD^+ + 3\ \text{phosphite} + \text{glucose} \rightarrow 2\ \text{ADP} + 3\ \text{NADH} + \text{glucose} - 6 - \text{phosphate}, \quad [6]$$

$$\text{ApdA: AMP} + NAD^+ + \text{phosphite} \rightarrow \text{ADP} + \text{NADH}. \quad [7]$$

Luciferase and hexokinase use exclusively ATP while pyruvate kinase uses only ADP, and all three reactions are considered to be irreversible (Eqs. **2**–**4**). With luciferase as auxiliary enzyme, light (and thus ATP), was produced only if the ApdA reaction (Eq. **7**) and myokinase reaction (Eq. **1**) were combined (Eq. **5**) (Fig. 2*B*). The only enzyme in the in vitro experiments of this study that truly enhanced the activity of ApdA was myokinase. Myokinase reacts reversibly into an equilibrium of ATP and AMP with 2 ADP (Eq. **1**) and possibly enables as such the ApdA reaction by withdrawing reaction product(s) from ApdA: We observed that ApdA in the absence of auxiliary enzymes produced at the very least micromolar concentrations of ADP when artificially high substrate concentrations were used (20 mM each), but also some ATP formation was detected (*SI Appendix*, Figs. S5 and S6), and we thus conclude that

The tight functional dependence of ApdA on auxiliary ADP- and/or ATP-consuming reactions as observed in our in-vitro

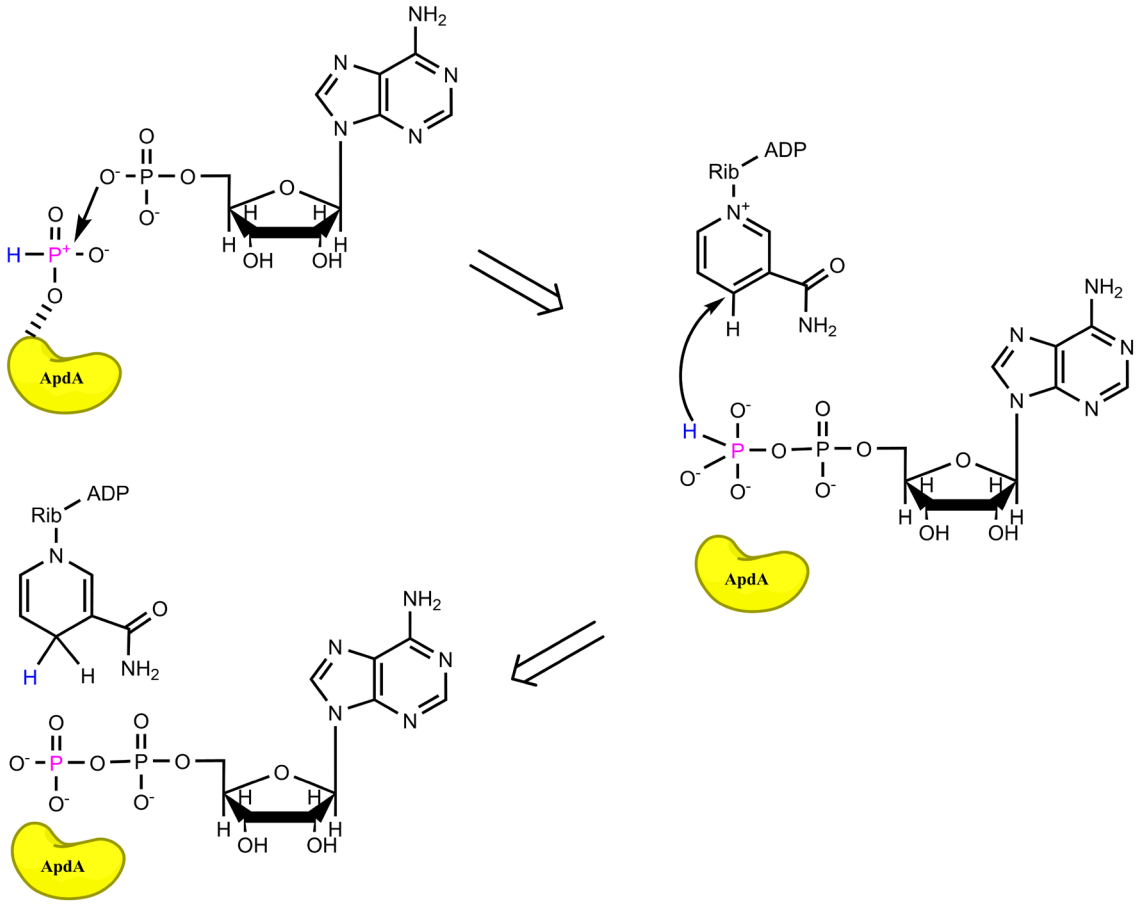

Fig. 5. Suggested reaction mechanism of phosphite oxidation by AMP-dependent phosphite dehydrogenase ApdA. The yellow object represents the enzyme.

enzyme experiments emphasizes that this type of substrate-level phosphorylation with phosphite may also in *P. fastidiosa* be dependent on a tight coupling with its ATP-consuming anabolic reactions during growth (45). Such a challenge of catalyzing phosphite-driven substrate-level phosphorylation might further be reflected in the considerable investment of *P. fastidiosa* into the biosynthesis of ApdA, being the most abundant protein in these cells and, hence, providing for a high amount of catalyst for this reaction to proceed efficiently in situ.

For phosphite oxidation by the unusual enzymes described in this study, we propose a reaction mechanism as shown in Fig. 5. First, the enzyme associates with the oxygen atom of phosphite; then, electrons are transferred from the phosphorus atom to the double bond of oxygen. Second, the oxygen atom of AMP attacks the central phosphorus atom of phosphite. Finally, the hydrogen atom leaves the phosphite residue as a hydride to NAD^+, to form NADH, which is reoxidized through the Wood–Ljungdahl pathway (*SI Appendix*, Fig. S12). ADP, ATP, and NADH thus formed are used mainly for synthesis of cell matter; in *D. phosphitoxidans*, some electrons can also flow into reduction of sulfate to sulfide. All enzymes necessary for cell matter synthesis from carbon dioxide through the Wood–Ljungdahl pathway were identified in the proteome and genome of both bacteria.

In conclusion, the ApdA enzymes described here are homologues to nucleotide-diphosphate-sugar epimerases of the SDR superfamily of NAD(P)-dependent oxidoreductases. Binding of the NAD cofactor in these enzymes is highly conserved and likely to be identical in both ApdA enzymes. Although the UDP-sugar-binding lobe is also well conserved, a notable change of a phosphate-coordinating arginine into a small serine and the extended loop at the entry of the substrate-binding pocket may explain the altered substrate binding of the two ApdA enzymes. Furthermore, the loss of the catalytic triad serine and possible subsequent placement of an arginine into the active center may explain the lack of epimerase activity and the observed function described in this paper.

In the Archean period, phosphite was more widespread on Earth than it is today (3, 6). The dissimilatory phosphite oxidation in the two bacterial strains known so far may be a remnant of these times and may indicate that phosphite played an important role in the early development of life. Further, both phosphite-oxidizing bacteria use the Wood–Ljungdahl pathway (*SI Appendix*, Fig. S12) that is assumed to be the oldest pathway of autotrophic cell matter synthesis (46, 47). Our present study adds a further reaction to the existing models for formation of phosphoanhydride bonds (9). It may contribute to the development of our understanding of the early evolution of life on Earth and can perhaps provide potential chemical markers relevant to the detection of life also in extraterrestrial environments.

Materials and Methods

Cultivation. *P. fastidiosa* strain DYL19^T (DSM 112739, GDMCC 1.2680) was cultivated under strictly anoxic conditions in sulfide-reduced, bicarbonate-buffered freshwater mineral-salts medium with 10 mM sodium phosphite as the sole electron donor and with CO_2 as the electron acceptor and sole carbon source for growth, as previously described (29). *D. phosphitoxidans* strain FiPS-3 (DSM 13687, OCM 818) was grown with 10 mM sodium phosphite as the sole electron donor and CO_2 as the electron acceptor in sulfide-reduced, bicarbonate-buffered marine mineral-salt medium (27). Cultures were incubated unshaken in the dark at 30 °C for about 20 d. All *E. coli* strains used in this study were cultivated with LB-medium (10 g/L tryptone, 5 g/L yeast extract, and 10 g/L NaCl) in the presence of 50 or 100 μg/mL kanamycin to increase the plasmid copy number; aqueous 50 mg/mL kanamycin stocks were filter-sterilized.

Preparation of Cell-Free Extracts and Soluble Fraction (SF). Anaerobic cultures of *P. fastidiosa* or *D. phosphitoxidans* had a volume of 0.5 to 1 L and were harvested in the late exponential growth phase, i.e., at an OD_{600} of around maximally 0.3 for *P. fastidiosa* and maximally 0.6 for *D. phosphitoxidans*; this corresponds to dry weight concentration of approximately 75 mg/L for *P. fastidiosa* and 150 mg/L for *D. phosphitoxidans* (48). Harvested *P. fastidiosa* and *E. coli* cells were washed once with 25 mM N-(2-hydroxyethyl) piperazine-N′-(2-ethanesulfonic acid) (HEPES) buffer, pH 8.0 (adjusted with KOH), containing 3 mM $MgCl_2$, by centrifugation at 7,000 × g for 20 min at 4 °C. *D. phosphitoxidans* cells were washed once with 3-(N-morpholino) propanesulfonic acid (MOPS), pH 7.2 (NaOH adjusted), containing 3 mM $MgCl_2$ and 17 mM NaCl, by centrifugation at 7,000 × g at 4 °C. The cells were resuspended in 3 to 5 mL of the same buffer and then disrupted by three or four passages through a cooled French Press Cell (SLM Aminco, Cat. No. FA003, Urbana, IL) at 104 MPa pressure. After removal of cell debris and intact cells by centrifugation at 16,000 × g for 30 min at 4 °C, the soluble protein fraction was separated from the membrane fraction by ultracentrifugation at 104,000 × g for 30 min at 4 °C. Typical protein concentrations in SFs for *P. fastidiosa* were 2.8 mg/mL and for *D. phosphitoxidans* 7.9 mg/mL, as estimated by the Bradford assay.

Total Proteome Analysis and Database Search. For total proteome analysis of cell-free extracts of *P. fastidiosa*, samples were digested with trypsin and analyzed by mass spectrometry at the Proteomics Facility of the University of Konstanz (www.biologie.uni-konstanz.de/proteomics-centre/) and the peptide fingerprints matched against a local database of all predicted proteins of the JGI's isolate genome annotation as described previously (49–51). Mass spectrometry was done with a LTQ Orbitrap Discovery with an Eksigent 2D-nano HPLC (Thermo Fisher Scientific, Waltham, MA, United States) or a Q-Exactive HF mass spectrometer (Thermo Fisher Scientific, Bremen, Germany) interfaced with an Easy-nLC 1200 nanoflow liquid chromatography system (Thermo Scientific, Odense, Denmark). The peptide digests were reconstituted in 0.1% formic acid and loaded onto the analytical column (5 μm, 100 Å pore size C_{18} resin in a 75-μm i.d. x 15-cm-long piece of fused silica capillary, Acclaim PepMap100, Thermo Scientific). Peptides were resolved at a flow rate of 300 nL/min using a linear gradient of 6 to 40% solvent B (0.1% formic acid in 80% acetonitrile) over 75 min. Data-dependent acquisition with full scans in 350 to 1,500 *m/z* range was carried out using the Orbitrap mass analyzer at a mass resolution of 120,000 at 200 *m/z*. The 20 most intense precursor ions were selected for further fragmentation. Only peptides with charge states 2 to 6 were used, and dynamic exclusion was set to 30 s. Precursor ions were fragmented using higher-energy collision dissociation with a normalized collision energy set to 28%. Fragment ion spectra were recorded at a resolution of 15,000. The Mascot search engine (Matrix Science, London, United Kingdom) was used to match each peptide fingerprint against the protein database of the IMG-annotated draft genomes of *P. fastidiosa* (GOLD Analysis Project ID Ga0451573; IMG genome ID 2888950683) and of *D. phosphitoxidans* (GOLD Analysis Project ID Ga0012722; IMG genome ID 2523231053). Relative protein abundances were expressed by the peak area of the peptides of each protein measured by the Eksigent 2D-nano total ion count. The term "area" here refers to the mean value of the two or maximally three most intense peptide intensities per protein, if at least two peptides per protein were identified. If no peptide was identified, the area value of the corresponding protein was set to zero.

Molecular Cloning. Genes for ApdA of *P. fastidiosa* or *D. phosphitoxidans* were cloned into pET-28a(+) in-frame with the N-terminal 6xHis-tag by conventional cloning techniques, i.e., restriction digests and DNA-ligase reactions with genes amplified by PCR with Phusion Polymerase (New England Biolabs) and with the primers listed in *SI Appendix*, Table S1. In two separate constructs, the two *apdA* homologs were also cloned into pET-28a(+) as genes that were codon-optimized for *E. coli* and synthesized under contract with BioCat (Heidelberg, Germany, *SI Appendix*, Supporting Information Data S6). All constructs used in this study were transformed either into *E. coli* NovaBlue DE3 as storage strain and into *E. coli* Rosetta gami DE3 or *E. coli* Shuffle T7 as expression strains. Stock cultures of the strains were prepared by mixing 900 μL of LB-grown culture with 100 μL pure DMSO in cryotubes and frozen at −80 °C.

Overexpression and Purification of ApdA. Precultures for overexpression were prepared by removing a small aliquot of cell paste from the frozen stock solution of the respective expression strain with a pipette tip and transferred to a sterile, closed culture tube containing 5 mL LB medium with 100 μg/mL kanamycin. This

preculture was incubated overnight on an orbital shaker at 200 rpm and 37 °C. On the following day, 500 to 1,000 mL of MagicMedia autoinduction medium (Thermo Fisher Scientific Inc., Karlsruhe, Germany) and 100 μg/mL kanamycin was inoculated with the complete preculture in a 2-L baffle flask shaking overnight (between 16 and 20 h) on an orbital shaker at 200 rpm and 37 °C. All subsequent manipulations were done either under oxic conditions on a regular laboratory bench or anoxic conditions in an anoxic chamber under an atmosphere of 95% N_2/5% H_2 as described previously (48). Cultures were dispensed into sterile centrifugation vessels and harvested by centrifugation at 7,000 × g for 20 min at 4 °C using a F10-6x500y FiberLite rotor operated in a RC 5C Plus Sorvall centrifuge (Thermo Fisher Scientific Inc., Karlsruhe, Germany). Pellets were suspended in 3 mL lysis/binding buffer [25 mM HEPES-KOH, pH 8.0, 3 mM $MgCl_2$, 10% (v/v) glycerol, 20 mM imidazole]. The pH values of all purification buffers had to be readjusted to 8.0 after addition of the strongly alkaline imidazole. Bacteria were lysed by three passages through a French Pressure Cell (Aminco, Silver Spring, MD, United States) operated at 137 MPa as described before (48). The lysate was spun down in a table-top centrifuge for 1.5 mL tubes at maximum speed (14,100 × g, MiniSpinPlus centrifuge, Eppendorf, Hamburg, Germany) for 5 min at room temperature to remove nonlysed cells and debris. Thereafter, membrane particles were removed in an Optima MAX-TL ultracentrifuge with a TLA 110 rotor (Beckman Coulter GmbH, Krefeld, Germany) at 100,000 × g for 60 min and the supernatant transferred to either a glass vial with butyl rubber stopper (anoxic storage) or a 15 mL polypropylene tube (SARSTEDT AG & Co. KG, Nümbrecht, Germany) and termed SF. For one typical example, the protein concentration of the SF from a 1-L culture as measured by the bicinchoninic acid assay was 31.5 mg/mL in a volume of 12 mL, thus a total protein amount of 378 mg. All protein samples were stored on ice in between manipulations. For small-scale protein preparation, His spin trap centrifugation columns (Cytiva, Freiburg, Germany) were used according to the manufacturer's instructions and for larger-scale production, protein was purified with 1-mL His-Trap FF columns (Cytiva, Freiburg, Germany) operated manually with syringes. The SF (5 to 10 mL) was applied to the column with a flow rate of approximately 1 mL/min in 2 mL increments and flushing the column in between with lysis/binding buffer. The column flow through (FT) was collected and stored on ice. The column was flushed with 6 mL wash buffer (25 mM HEPES-KOH, pH 8.0, 3 mM $MgCl_2$, 10% (v/v) glycerol, and 40 mM imidazole), and the wash fraction (WA) was also collected and stored on ice. His-tagged protein was eluted from the column with 3 mL elution buffer [25 mM HEPES-KOH, pH 8.0, 3 mM $MgCl_2$, 10% (v/v) glycerol, and 400 mM imidazole]. The resulting protein preparation was termed ApdA and was stored on ice until further use.

Protein Gel Electrophoresis, Activity Staining, and Identification of Protein Bands. Precast SDS-PAGE gels were run at 30 mA per gel for 1 h on a BioRad Ready Strip IPG/Protean II system. Gels were stained with ReadyBlue Protein Gel Stain (Sigma-Aldrich). Enzyme activity staining was performed with Native-PAGE gels and cytoplasmic cell fractions under anoxic conditions (52). *P. fastidiosa* phosphite-oxidizing activity was stained by immersing the gel strips in 25 mM HEPES buffer, pH 8.0, containing 3 mM $MgCl_2$, and *D. phosphitoxidans* phosphite-oxidizing activity in 25 mM MOPS buffer, pH 7.2, containing 3 mM $MgCl_2$ and 17 mM NaCl, each with addition of 2 mM AMP, 2 mM NAD^+, 10 mM sodium phosphite, and 0.4 mM iodonitrotetrazolium chloride (INT) as the final electron acceptor in order to indirectly detect NADH formation. Protein bands excised from stained Native-PAGE gels and SDS-PAGE gels were identified by peptide mass fingerprinting at the Proteomics Facility of the University of Konstanz.

Photometric Enzyme Assays. Activity of ApdA was routinely measured in a V-630 spectrophotometer (Jasco, Pfungstadt, Germany) at 30 °C either under air in 1-mL polystyrene cuvettes (SARSTEDT AG & Co. KG, Nümbrecht, Germany) or under anoxic conditions in 1-mL Quartz cuvettes stoppered with natural rubber and flushed with 100% N_2. Enzyme kinetics were recorded at 340 nm following the formation of NADH from NAD^+ ($\varepsilon_{340} = 6.3\ mM^{-1}\ cm^{-1}$, 53). The Time Course Measurement software of the Jasco Spectra Manager software package, version 2.10.01, was used. Each 1 mL full-activity assay in 25 mM HEPES-KOH, pH 8.0, with 3 mM $MgCl_2$ consisted of 2 mM NAD^+, 2 mM AMP, 10 mM phosphite, 20 units myokinase (adenylate kinase), and approximately 200 to 250 μg ApdA enzyme applied in a 50 μL addition per 1 mL assay. In assays with pyruvate kinase or hexokinase as sole auxiliary enzymes, myokinase was omitted and 2 mM PEP plus 20 units pyruvate kinase or 20 mM glucose plus 20 units hexokinase was added. Additions were made either by micropipettes or by syringes and needles (Hamilton, Bonaduz, Switzerland). For negative controls, individual compounds were omitted as indicated in the Results section. Small aliquots of ApdA were denatured at 99 °C for 5 min and added to enzyme assays to test for background reactions (heat-inactivated control). In additional assays, the reversibility of the enzyme activity was tested by observing NADH depletion at 340 nm or 365 nm. Data of each time course measurement were transferred to the Spectra Analysis software implemented in the Spectra Manager package, and the slope of each measurement (absorption per min) was calculated with the Kinetics tool.

Discontinuous Enzyme Assays. For discontinuous quantification of reactants, 2 mL or 3 mL assays were prepared either in oxic plastic tubes or in anoxic glass vials with butyl rubber stoppers flushed with 100% N_2 at 30 °C. The assay mixture contained the same components as for the photometric enzyme assays described above or, where indicated, increased substrate concentrations (20 mM NAD^+, 20 mM AMP, and 20 mM phosphite) in order to allow detection of products formed by ApdA in the absence of auxiliary enzymes. In experiments with increased substrate concentrations, direct 20-μL injections into the HPLC system were made from assay mixtures set up in HPLC vials. In all other experiments, and where indicated, assays were sampled before and after addition of ApdA, and the respective loss in volume was compensated by addition of assay buffer. At specific time intervals, 200 μL or 300 μL samples were withdrawn with either micropipettes or syringes and transferred to a 1.5 mL tube. For analysis of AMP, ADP, ATP, phosphite, and phosphate, 100 μL samples were mixed with 10 μL of 350 mM H_2SO_4 to denature protein by acidification. Precipitated protein was partially removed by centrifugation in a table-top centrifuge at 14,100 x g for 5 to 10 min. Supernatants were transferred to HPLC vials with crimp septa and analyzed as outlined below. Calibration standards were treated in the same way. Control samples with the nucleoside phosphates in buffer or water with or without prior acidification exhibited only minor variations even after prolonged storage in the autosampler at room temperature, indicating that these compounds were stable under slightly acidic conditions. The remaining 100 μL sample was used for NADH analysis by mixing with 900 μL oxic assay buffer and measuring the absorbance at 340 nm in a Jasco V-730 spectrophotometer with Fixed Wavelength Measurement software of the Spectra Manager package, version 2.14.06 (Jasco, Pfungstadt, Germany).

Analytical Procedures. Nucleoside phosphates (AMP, ADP, ATP) were analyzed by reversed-phase HPLC on a LiChrosorb RP18-5 column, 250 × 4.6 mm (Merck) fitted with a C-12 guard column (Phenomenex, Aschaffenburg, Germany) as described previously (54). A Shimadzu Prominence HPLC system consisting of two gradient pumps (LC-20AT), an autosampler (SIL-20A), a PDA-detector (SPD-M20A), an oven at 25 °C (CTO-10ACvp), and operated with the LCsolution software version 1.25, was used (Shimadzu, Munich, Germany). Each chromatography run was performed isocratically with 100% solvent A (potassium phosphate buffer, 0.1 M, pH 6.0, containing 4% methanol or, where indicated, 3% methanol in ultrapure water) for 13 min at a flow of 1 mL/min. Then, the concentration of solvent B (100% methanol) was raised to 50% within 0.1 min and maintained at 50% for 2.5 min, in order to clean the column in between runs, followed by re-equilibration of the column for 2.5 min with 100% solvent A. Thereafter, the flow was stopped for 1 min to allow for decompression of the resin; this helped to improve the reproducibility of retention times. Each 10 μL of sample or standards was injected.

Luciferase assays were performed with an ATP Determination Kit PRO (Biaffin GmbH & Co KG, Kassel, Germany). Assay working reagents consisting of reaction buffer, DTT, D-Luciferin, and firefly luciferase were prepared according to the manufacturer's instructions. ApdA assays and the corresponding controls were set up in a total volume of 1 mL each in HEPES buffer and with the same concentrations as described in the enzyme assay method section. Each 50 μL assay mixture or control was transferred to a well of a white bottom 96-well plate (ThermoFisher Scientific/Nunc A/S, Roskilde, Denmark), and immediately thereafter, 50 μL luciferase assay working reagent was added to each well, thus reducing the ApdA-assay reagents concentrations by 50%. The plate was shaken for 30 s in a SpectraMax iD3 plate reader operated with the SoftMax Pro 7.1 software (Molecular Devices GmbH, München, Germany), and the chemiluminescence of triplicate, lidded wells was recorded at 560 for 62 min in 2-min intervals.

Phosphite and phosphate were analyzed with Rezex™ RHM-Monosaccharide HC (8%) ion exchange resin (LC column 300 mm × 7.8 mm, 00H-0132-K0,

Phenomenex, Aschaffenburg, Germany) with 30 mM H_2SO_4 in ultrapure water as the mobile phase on an HPLC system equipped with a refractive index detector as described before (55). Each 20 μL of sample or standard was injected.

Protein concentrations were estimated by either the Bradford assay (56) with bovine serum albumin as standard, or the Pierce BCA Protein Assay Kit according to the manufacturer's manual (Thermo Fisher Scientific Inc., Karlsruhe, Germany).

Protein purity was assessed by SDS-PAGE using the Mini-PROTEAN 3 System (Bio-Rad Laboratories GmbH, Feldkirchen, Germany) and 4 to 15% Mini-PROTEAN TGX™ precast gradient protein gels, 10-well, 30 μL, according to the manufacturer's manuals. Samples (5, 10, or 20 μL) were mixed with 50 μL SDS-loading dye with β-mercaptoethanol as the reducing agent in at least equal volumes and incubated at 99 °C for 5 min in a Thermomixer comfort (Eppendorf, Hamburg, Germany). After cooling on ice, 5 to 20 μL of these samples was loaded on the gels and run for 55 min at 20 mA per gel. Gels were removed from the gel cassette, rinsed in deionized water for at least 5 min to remove SDS, and stained with ReadyBlue Protein Gel Stain (Merck/Sigma-Aldrich, Darmstadt, Germany) for 2 h to overnight on a rocking shaker. Stained gels were imaged with an HP Scanjet G4050 scanner at a resolution of 600 dpi against a white background and with auto-adjustments of the software turned off. Scanned images were saved as JPEG files, cropped, and labelled without manipulating contrast or brightness.

Analysis of Sequence Conservation. To identify homologues of the ApdA enzymes with known 3D-structure, the sequence of these enzymes was used in a search of the Protein Data Bank (PDB; https://www.rcsb.org) using BLAST (57) as search engine. Of the top hits, the following structures were selected as they had the highest sequence similarity to the *P. fastidiosa* ApdA: *P. shigelloides* UDP-GalNAc 4-epimerase (UniProtKBQ7BJX9), *M. thermautotrophicus* UDP-GalNAc 4-epimerase (UniProtKB O26475), *Bacillus thuringiensis* Pal (UniProtKB Q3ESA4), *T. maritima* UDP-glucose 4-epimerase (UniProtKB Q9WYX9), *M. tuberculosis* UDP-glucose 4-epimerase GalE1 (UniProtKB P9WN67). Their sequences were then aligned using Clustal omega (58).

To identify the conservation of residue 212 the *P. fastidiosa* ApdA, the sequence was used to identify protein homologs from the nonredundant protein database in the BLAST webserver (57). The position was examined for the top 100 homologous sequences (which included *Dp*ApdA). Residues involved in substrate interactions were determined using the annotation in the sequence inspector of the PDB (59), confirmed through visual inspection of 3D-structures in UCSF Chimera (60).

Prediction of 3D Models using AlphaFold. 3D models of the ApdA enzyme of *P. fastidiosa* (NCBI entry WP_231685625.1) and of *D. phosphitoxidans* (UniProtKB S0G1B2) were predicted using AlphaFold version 2.1.1 (38). AlphaFold calculations were executed at the University of Konstanz on a customized computer server (consisting of a processor AMD Ryzen Threadripper Pro 3975 wx equipped with graphics card Nvidia GForce RTX 3090 and 256GB RAM running the Ubuntu 20.04.4 operative system). The template database included entries at the Protein Data Bank up to 22-12-2021. For each sequence, six models were calculated, and the relaxed model 0 was chosen for further analysis. The geometry of the resulting models was validated using Molprobity (61).

Chemicals. Auxiliary enzymes myokinase from yeast (adenylate kinase lyophilized powder, 475941), pyruvate kinase from rabbit muscle (type VII, P7768), and hexokinase from *Saccharomyces cerevisiae* (type F-300, H4502) were purchased from Merck/Sigma-Aldrich (Schnelldorf, Germany). All other chemicals were obtained from the same company or from Carl Roth GmbH + Co. KG (Karlsruhe, Germany) and were of analytical grade quality.

Data, Materials, and Software Availability. All study data are included in the article and/or supporting information.

ACKNOWLEDGMENTS. We are indebted to Prof. Dr. Wolfgang Buckel who contributed early an idea for the reaction mechanism of ApdA. Portions of this work were developed from the doctoral thesis of Zhuqing Mao. We thank the Deutscher Akademischer Austauschdienst for providing a scholarship to Zhuqing Mao, within the program of the Konstanz Research School Chemical Biology at the University of Konstanz. We are grateful to Prof. Dr. Peter Kroneck and to Prof. Dr. Jörg Hartig for helpful discussions and suggestions. Our gratitude goes also to Prof. Dr. Kay Diederichs and Dr. Karsten Schäfer for the provision of computing infrastructure and scientific support in the prediction of models using AlphaFold, and for proteome analysis done by Dr. Andreas Marquardt at the Proteomics Center of the University of Konstanz. We thank Sylke Wiechmann and Julia Schmidt for technical support. Zhuqing Mao is grateful for support by Duan Yuanling. Helena Pfingst and Lena Schulz helped with enzyme preparation and enzyme assays as part of a practical class of the AG Schleheck.

Author affiliations: [a]Department of Biology, University of Konstanz, Constance 78457, Germany; and [b]Konstanz Research School Chemical Biology, Departments of Chemistry and Biology, University of Konstanz, Constance 78457, Germany

1. J. Emsley, *Shocking History of Phosphorus: A Biography of the Devil's Element* (MacMillan, London, 2001), p. 336.
2. N. Wiberg, *Hollemann-Wiberg's Lehrbuch der anorganischen Chemie* (Walter de Gruyter, Berlin, ed. 33, 1985).
3. M. A. Pasek, J. P. Harnmeijer, R. Buick, M. Gull, Z. Atlas, Evidence for reactive reduced phosphorus species in the early Archean ocean. *Proc. Natl. Acad. Sci. U.S.A.* **110**, 10089–10094 (2013).
4. C. Deduve, The beginnings of life on earth. *Am. Sci.* **83**, 428–437 (1995).
5. B. Schink, Biological cycling of phosphorus. *Met. Ions Biol. Syst.* **43**, 131–151 (2005).
6. M. A. Pasek, J. M. Sampson, Z. Atlas, Redox chemistry in the phosphorus biogeochemical cycle. *Proc. Natl. Acad. Sci. U.S.A.* **111**, 15468–15473 (2014).
7. B. L. Hess, S. Piazolo, J. Harvey, Lightning strikes as a major facilitator of prebiotic phosphorus reduction on early Earth. *Nat. Commun.* **12**, 1535 (2021).
8. I. A. Figueroa, J. D. Coates, Microbial phosphite oxidation and its potential role in the global phosphorus and carbon cycles. *Adv. Appl. Microbiol.* **98**, 93–117 (2017).
9. M. A. Pasek, Thermodynamics of prebiotic phosphorylation. *Chem. Rev.* **120**, 4690–4706 (2020).
10. B. Herschy *et al.*, Archean phosphorus liberation induced by iron redox geochemistry. *Nat. Commun.* **9**, 1346 (2018).
11. C. J. Lovatt, R. L. Mikkelsen, Phosphite fertilizers: What are they? Can you use them? What can they do? *Better Crops* **90**, 11–13 (2006).
12. H. T. B. Thao, T. Yamakawa, Phosphite (phosphorous acid): Fungicide, fertilizer or bio-stimulator? *Soil Sci. Plant Nutr.* **55**, 228–234 (2009).
13. S. Rossall, C. Qing, M. Paneri, M. Bennett, R. Swarup, A "growing" role for phosphites in promoting plant growth and development. *Acta Hortic* **1148**, 61–67 (2016).
14. W. W. Metcalf, R. S. Wolfe, Molecular genetic analysis of phosphite and hypophosphite oxidation by *Pseudomonas stutzeri* WM88. *J. Bacteriol.* **180**, 5547–5558 (1998).
15. F. Adams, J. P. Conrad, Transition of phosphite to phosphate in soils. *Soil Sci.* **75**, 361–371 (1953).
16. L. E. Casida, Microbial oxidation and utilization of orthophosphite during growth. *J. Bacteriol.* **80**, 237–241 (1960).
17. G. M. Malacinski, W. A. Konetzka, Bacterial oxidation of orthophosphite. *J. Bacteriol.* **91**, 578–582 (1966).
18. G. M. Malacinski, W. A. Konetzka, Orthophosphite-nicotinamide adenine dinucleotide oxidoreductase from *Pseudomonas fluorescens*. *J. Bacteriol.* **93**, 1906–1910 (1967).
19. W. Heinen, A. M. Lauwers, Hypophosphite oxidase from *Bacillus caldolyticus*. *Arch. Microbiol.* **95**, 267–274 (1974).
20. T. L. Foster, L. Winans, S. J. S. Helms, Anaerobic utilization of phosphite and hypophosphite by *Bacillus* sp. *Appl. Environ. Microb.* **35**, 937–944 (1978).
21. W. W. Metcalf, B. L. Wanner, Involvement of the *Escherichia coli* Phn (*psiD*) gene-cluster in assimilation of phosphorus in the form of phosphonates, phosphite, Pi esters, and Pi. *J. Bacteriol.* **173**, 587–600 (1991).
22. K. Imazu *et al.*, Enhanced utilization of phosphonate and phosphite by *Klebsiella aerogenes*. *Appl. Environ. Microbiol.* **64**, 3754–3758 (1998).
23. A. M. Costas, A. K. White, W. W. Metcalf, Purification and characterization of a novel phosphorus-oxidizing enzyme from *Pseudomonas stutzeri* WM88. *J. Biol. Chem.* **276**, 17429–17436 (2001).
24. J. M. Vrtis, A. K. White, W. W. Metcalf, W. A. van der Donk, Phosphite dehydrogenase: An unusual phosphoryl transfer reaction. *J. Am. Chem. Soc.* **123**, 2672–2673 (2001).
25. K. C. Yang, W. W. Metcalf, A new activity for an old enzyme: *Escherichia coli* bacterial alkaline phosphatase is a phosphite-dependent hydrogenase. *Proc. Natl. Acad. Sci. U.S.A.* **101**, 7919–7924 (2004).
26. B. Schink, M. Friedrich, Phosphite oxidation by sulphate reduction. *Nature* **406**, 37 (2000).
27. B. Schink, V. Thiemann, H. Laue, M. W. Friedrich, *Desulfotignum phosphitoxidans* sp. nov., a new marine sulfate reducer that oxidizes phosphite to phosphate. *Arch. Microbiol.* **177**, 381–391 (2002).
28. D. D. Simeonova, M. M. Wilson, W. W. Metcalf, B. Schink, Identification and heterologous expression of genes involved in anaerobic dissimilatory phosphite oxidation by *Desulfotignum phosphitoxidans*. *J. Bacteriol.* **192**, 5237–5244 (2010).
29. Z. Mao *et al.*, *Phosphitispora fastidiosa* gen. nov. sp. nov., a new dissimilatory phosphite-oxidizing anaerobic bacterium isolated from anaerobic sewage sludge. *Int J. Syst. Evol. Microbiol.* **71**, 1–7 (2021).
30. W. Buckel, Inorganic chemistry in marine sediments. *Angew. Chem. Int. Ed. Engl.* **40**, 1417–1418 (2001).
31. I. A. Figueroa *et al.*, Metagenomics-guided analysis of microbial chemolithoautotrophic phosphite oxidation yields evidence of a seventh natural CO_2 fixation pathway. *Proc. Natl. Acad. Sci. U.S.A.* **115**, E92–E101 (2018).
32. S. D. Ewens *et al.*, The diversity and evolution of microbial dissimilatory phosphite oxidation. *Proc. Natl. Acad. Sci. U.S.A.* **118**, e2020024118 (2021).
33. Z. Mao, "AMP-dependent phosphite dehydrogenase, a key enzyme in dissimilatory phosphite oxidation", Thesis, University of Konstanz, Konstanz, Germany (2022).
34. D. D. Simeonova, J. Susnea, A. Moise, B. Schink, M. Przybylski, "Unknown genome" proteomics: A new NAD(P)-dependent epimerase/dehydratase revealed by N-terminal sequencing, inverted PCR, and high resolution mass spectrometry. *Mol. Cell. Proteomics* **8**, 122–131 (2009).

35. A. Poehlein, R. Daniel, B. Schink, D. D. Simeonova, Life based on phosphite: A genome-guided analysis of *Desulfotignum phosphitoxidans*. *BMC Genomics* **14**, 753 (2013).
36. K. L. Kavanagh, H. Jornvall, B. Persson, U. Oppermann, Medium- and short-chain dehydrogenase/reductase gene and protein families: The SDR superfamily–functional and structural diversity within a family of metabolic and regulatory enzymes. *Cell Mol. Life Sci.* **65**, 3895–3906 (2008).
37. P. A. Frey, A. D. Hegeman, Chemical and stereochemical actions of UDP-galactose 4-epimerase. *Acc Chem. Res.* **46**, 1417–1426 (2013).
38. J. Jumper *et al.*, Highly accurate protein structure prediction with AlphaFold. *Nature* **596**, 583–589 (2021).
39. Y. Liu *et al.*, Mechanistic roles of tyrosine 149 and serine 124 in UDP-galactose 4-epimerase from *Escherichia Coli*. *Biochemistry* **36**, 10675–10684 (1997).
40. J. D. King *et al.*, Predicting protein function from structure – the roles of short-chain dehydrogenase/reductase enzymes in *Bordetella* O-antigen biosynthesis. *J. Mol. Biol.* **374**, 749–763 (2007).
41. R. K. Thauer, K. Jungermann, K. Decker, Energy conservation in chemotrophic anaerobic bacteria. *Bacteriol. Rev.* **41**, 100–180 (1977).
42. S. Su, P. J. Russell, Adenylate kinase from baker's yeast. II. Substrate specificity. *Biochim. Biophys. Acta* **132**, 370–378 (1967).
43. C. Boehme *et al.*, Chemical and enzymatic characterization of recombinant rabbit muscle pyruvate kinase. *Biol. Chem.* **394**, 695–701 (2013).
44. R. E. Viola, F. M. Raushel, A. R. Rendina, W. W. Cleland, Substrate synergism and the kinetic mechanism of yeast hexokinase. *Biochemistry* **21**, 1295–1302 (1982).
45. Z. Mao, N. Müller, S. Borusak, D. Schleheck, B. Schink, Anaerobic dissimilatory phosphite oxidation, an extremely efficient concept of microbial electron economy. *Environ. Microbiol.*, 1–7 (2023).
46. W. F. Martin, Older than genes: The acetyl CoA pathway and origins. *Front. Microbiol.* **11**, 817 (2020).
47. J. C. Xavier *et al.*, The metabolic network of the last bacterial common ancestor. *Commun. Biol.* **4**, 413 (2021).
48. A. Keller, B. Schink, N. Müller, Energy-conserving enzyme systems active during syntrophic acetate oxidation in the thermophilic bacterium *Thermacetogenium phaeum*. *Front. Microbiol.* **10**, 2785 (2019).
49. A. K. Felux, D. Spiteller, J. Klebensberger, D. Schleheck, Entner-Doudoroff pathway for sulfoquinovose degradation in *Pseudomonas putida* SQ1. *Proc. Natl. Acad. Sci. U.S.A.* **112**, E4298–E4305 (2015).
50. S. C. Peck *et al.*, A glycyl radical enzyme enables hydrogen sulfide production by the human intestinal bacterium *Bilophila wadsworthia*. *Proc. Natl. Acad. Sci. U.S.A.* **116**, 3171–3176 (2019).
51. X. Xie, D. Spiteller, T. Huhn, B. Schink, N. Müller, *Desulfatiglans anilini* initiates degradation of aniline with the production of phenylphosphoamidate and 4-aminobenzoate as intermediates through synthases and carboxylases from different gene clusters. *Front. Microbiol.* **11**, 2064 (2020).
52. A. Schmidt, N. Müller, B. Schink, D. Schleheck, A proteomic view at the biochemistry of syntrophic butyrate oxidation in *Syntrophomonas wolfei*. *PLoS One* **8**, e56905 (2013).
53. J. Ziegenhorn, M. Senn, T. Bucher, Molar absorptivities of beta-NADH and beta-NADPH. *Clin. Chem.* **22**, 151–160 (1976).
54. G. Leoncini, E. Buzzi, M. Maresca, M. Mazzei, A. Balbi, Alkaline extraction and reverse-phase high-performance liquid chromatography of adenine and pyridine nucleotides in human platelets. *Anal. Biochem.* **165**, 379–383 (1987).
55. A. Keller, B. Schink, N. Müller, Alternative pathways of acetogenic ethanol and methanol degradation in the thermophilic anaerobe *Thermacetogenium phaeum*. *Front. Microbiol.* **10**, 423 (2019).
56. M. M. Bradford, A rapid and sensitive method for the quantitation of microgram quantities of protein utilizing the principle of protein-dye binding. *Anal. Biochem.* **72**, 248–254 (1976).
57. C. Camacho *et al.*, BLAST+: Architecture and applications. *BMC Bioinformatics* **10**, 421 (2009).
58. F. Sievers *et al.*, Fast, scalable generation of high-quality protein multiple sequence alignments using Clustal Omega. *Mol. Syst. Biol.* **7**, 539 (2011).
59. H. M. Berman *et al.*, The protein data bank. *Nucleic Acids Res.* **28**, 235–242 (2000).
60. E. F. Pettersen *et al.*, UCSF Chimera–a visualization system for exploratory research and analysis. *J. Comput. Chem.* **25**, 1605–1612 (2004).
61. C. J. Williams *et al.*, MolProbity: More and better reference data for improved all-atom structure validation. *Protein Sci.* **27**, 293–315 (2018).